

---

# 2

## Axial segregation in high intensity discharge lamps measured by laser absorption spectroscopy

---

**Abstract.**

High intensity discharge lamps have a high efficiency. These lamps contain rare-earth additives (in our case dysprosium iodide) which radiate very efficiently. A problem is colour separation in the lamp because of axial segregation of the rare-earth additives, caused by diffusion and convection. Here two-dimensional atomic dysprosium density profiles are measured by means of laser absorption spectroscopy; the order of magnitude of the density is  $10^{22} \text{ m}^{-3}$ . The radially resolved atomic density measurements show a hollow density profile. In the outer parts of the lamp molecules dominate, while the centre is depleted of dysprosium atoms due to ionization. From the axial profiles the segregation parameter is determined. It is shown that the lamp operates on the right-hand side of the Fischer curve [J. Appl. Phys. **47**, 2954 (1976)]; a larger convection leads to less segregation.

---

This chapter has been adapted from [A.J. Flikweert, T. Nimalasuriya, C.H.J.M. Groothuis, G.M.W. Kroesen, and W.W. Stoffels, *Axial segregation in high intensity discharge lamps measured by laser absorption spectroscopy*, J. Appl. Phys. **98** (2005) 073301].

## 2.1 Introduction

The goal of this research is to gain a better understanding of the metal-halide lamp (MH, which is a High Intensity Discharge lamp, HID) [3] with a high efficiency (up to 40%), so that it can be improved. These lamps contain usually mercury as buffer gas and often rare-earth additives which radiate very efficiently in the visible spectrum. Ideally the lamp radiates white light, but when the lamp burns vertically, colour separation takes place because of segregation of the rare-earth additives. A picture of the colour separation is shown in figure 2.1.

The colour separation is caused by a combination of radial and axial segregations; the latter is caused by the combination of convection and diffusion [21–25]. E. Fischer [28] has formulated a simplified theory explaining the segregation based on the diffusion and convection in the lamp. Convection is caused by gravity and in order to understand its influence the lamp has recently been investigated under micro-gravity conditions so that no convection flows were present. To obtain micro-gravity, experiments during parabolic flights and at the International Space Station have been performed.

To get more insight in the flow phenomena and the segregation in the lamp, we present absorption measurements of atomic dysprosium. From this a two-dimensional density profile of the rare-earth atoms is obtained. We want to understand the theory about radial and axial segregations (depicted by E. Fischer) quantitatively by means of a model and experimental verification.

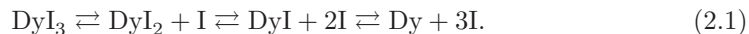
First we briefly introduce the theory of diffusion, convection, and axial segregation in the lamp. Next absorption spectroscopy is discussed and the experimental setup is presented. Finally the results of measurements on a lamp for two different input powers is given; the density profiles are shown and the segregation parameters are obtained from these profiles.

## 2.2 Theory

The segregation theory on MH lamps has been invented by E. Fischer [28]. It will be briefly summarized here for our specific case of a  $\text{DyI}_3$  containing lamp (burner height 20 mm, diameter of 8 mm).

### 2.2.1 Radial segregation

The centre of the burner is much hotter ( $\sim 5500$  K) than the wall ( $\sim 1200$  K) [29]. Because of this large temperature gradient a multi-step process of dissociation of  $\text{DyI}_3$  molecules near the centre and association of atoms at the wall takes place [30]:



With increasing temperature the equilibrium moves to the right-hand side. Furthermore in the centre of the burner ionization of Dy atoms takes place because of the high



**Figure 2.1:** (printed in colour in figure 1.3) Picture of a HID lamp burner (real size 8 mm x 20 mm); colour separation is clearly visible.

temperature [31]:



The diffusion velocities of atoms, molecules and ions are different. Due to the different velocities the particles in the hotter part diffuse faster than the particles in the colder part. This results in a hollow profile of the elemental density of dysprosium; this is called radial segregation. Elemental density means that contributions from all molecules, atoms and ions of a particular element are included. Note that this is in addition to the ideal gas law  $p = nkT$ ; a higher temperature gives a lower density.

### 2.2.2 Convection and axial segregation

In addition to radial segregation, the radial temperature gradient is related to convection in the lamp. The gas in the hot centre moves upwards whereas the gas at the wall moves downwards. As discussed in section 2.2.1, the maximum of the elemental Dy density lies in the part where the gas moves downward. This causes the Dy density to be higher near the bottom than near the top of the burner: axial segregation occurs [21, 22]. A picture of the diffusion and convection flows of the atoms and molecules is given in figure 2.2.

The simple axial segregation model by E. Fischer results in an exponential decrease of the axial Dy density  $n_{\text{Dy}}(z)$  with increasing height in the plasma [28]:

$$n_{\text{Dy}}(z) = n_{\text{Dy},0} \exp(-\lambda z), \quad (2.3)$$

where the axial segregation is described by the segregation parameter  $\lambda$  and  $n_{\text{Dy},0}$  is the atomic dysprosium density at the bottom of the lamp.

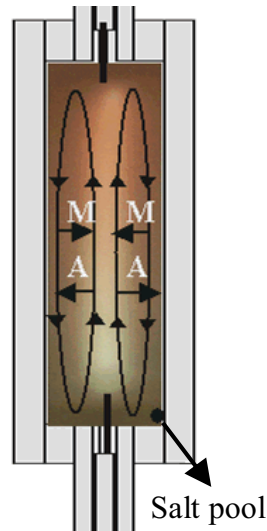


**Figure 2.2:** Schematic view of the burner in a HID lamp; diffusion and convection of atoms ( $A$ ) and molecules ( $M$ ) are indicated by arrows.

As explained, axial segregation is due to the combined effect of radial segregation and axial convection. In the absence of convection, or in the limit of extremely high convection speeds, there is no axial segregation and consequently the segregation parameter  $\lambda$  is zero (no axial colour separation). In the intermediate region  $\lambda$  has a maximum. This is depicted by the so-called Fischer curve [28], shown in figure 2.3, which gives the dependence of  $\lambda$  on the amount of convection inside the lamp. The amount of convection increases with the pressure in the lamp (Fischer), the input power [23, 24],<sup>1</sup> the gravity [43], and radius of the burner.

### 2.3 Experimental setup

To get insight into axial and radial segregations, the absolute number density of ground state atomic dysprosium is measured by means of laser absorption spectroscopy.

The lamp that is measured is shown schematically in figure 2.4. It contains 10 mg of mercury as buffer gas, 300 mbar Ar/Kr as starting gas and 4.2 mg DyI<sub>3</sub> as salt additive. The lamp driver that is used (Philips HID-DynaVision type LA 03 07)

<sup>1</sup>Nimalasuriya *et al* [41] observed more contraction when the power is increased, leading to a higher axis temperature and a higher convection speed. In addition, the radial segregation increases with increasing power, which leads to a stronger axial segregation.

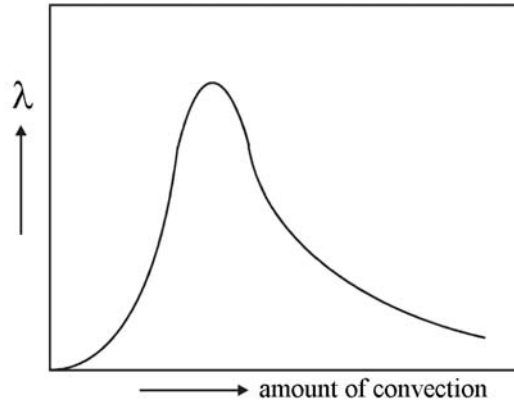


**Figure 2.3:** The Fischer curve, giving the dependence of the segregation parameter  $\lambda$  (equation (2.3)) on the convection in the lamp.

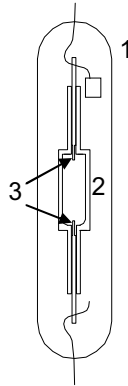


**Figure 2.4:** Schematic picture of the HID lamp: (1) outer bulb; (2) burner with height 20 mm and diameter 8 mm; (3) electrodes, distance between both electrodes  $\sim 18$  mm.

delivers a square-wave current to the lamp with a frequency of 125 Hz. The lamp is measured at two different input powers (113.5 and 151 W) to see the dependence of segregation on the input power. The input power is determined by using a power analyzer (Lem Norma 3000).

A diode laser (Sacher TEC 500 645-5, typical line width  $\leq 2$  MHz or  $\leq 3$  fm) scans a small wavelength range (0.14 nm) around the absorption wavelength  $\lambda = 642.19$  nm (transition from ground state  $[\text{Xe}].4f^{10}6s^2\ ^5I_8$  to excited state  $[\text{Xe}].4f^{10}(\ ^5I_8)6s6p(\ ^3P_0)$

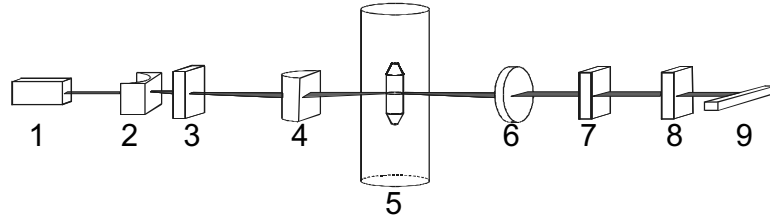


**Figure 2.5:** Schematic overview of the absorption setup to measure the ground state Dy density in a HID lamp: (1) diode laser; (2) cylindrical lens  $f = -12.7$  mm; (3) slit; (4) cylindrical lens  $f = +62.9$  mm; (5) lamp; (6) spherical lens  $f = +100$  mm; (7) slit; (8) interference filter; (9) diode array.

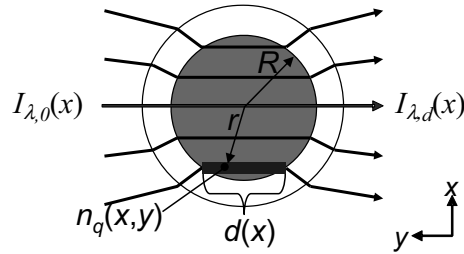


**Figure 2.6:** The laser beam  $I_{\lambda,0}$  enters the inner bulb as a parallel beam. Inside the plasma with boundary  $R$  it is partially absorbed;  $I_{\lambda,d}$  is the transmitted laser beam at the lateral position  $x$ . The local dysprosium density  $n_q(x,y) = n_q(r)$  is indicated; however laser absorption samples the integrated line of sight  $d(x)$  or column density.

(8,0)<sub>8</sub>) by changing the piezo voltage of the grating. The line strength of this transition is  $S = 6.65 \times 10^{-9} \text{ m}^2\text{C}^2$  [44, 45]. The line strength is related to the oscillator strength  $f_{qp}$  by  $S = (3g_q h e^2 \lambda) / (8\pi^2 m_e c) \times f_{qp}$  where  $g_q$  is the allowed number of states of the ground level  $q$ . The line is pressure broadened<sup>2</sup> with an experimentally determined width of around 40 pm.

A schematic overview of the setup for laser absorption on a HID lamp is given in figure 2.5. The laser beam (beam height  $\sim 1$  mm) passes two cylindrical lenses; in this way the laser spot is transformed to a parallel sheet inside the lamp burner. The width of the slit (no. 3 in the picture) is chosen so that exactly the whole width of the burner is illuminated. The inner and outer bulbs of the lamp act as negative cylindrical lenses. The beam passes the plasma in the burner as is shown in figure 2.6. Also indicated are the laser intensity  $I_{\lambda,0}(x)$  in the absence of the plasma and the laser intensity  $I_{\lambda,d}(x)$

<sup>2</sup>The mechanism is Van der Waals broadening [46] between Dy and Hg atoms, which leads to a Lorentzian line shape.

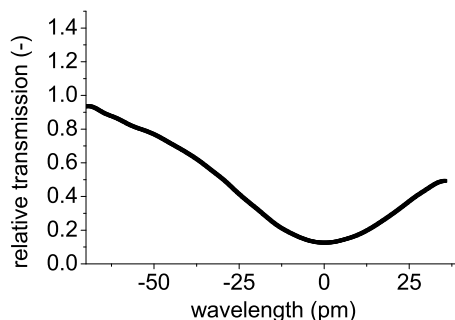


**Figure 2.7:** Typical relative transmission curve (lamp-on  $I_{\lambda,0}(x)$  divided by lamp-off  $I_{\lambda,d}(x)$ ) at a certain position  $x$ ; the wavelength is relative to the absorption wavelength (642.19 nm).

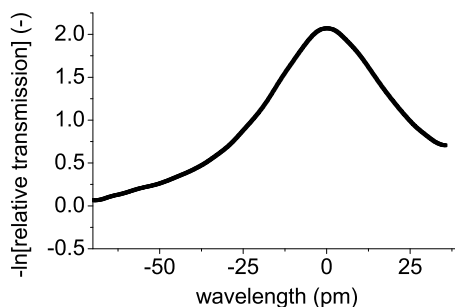


**Figure 2.8:** Logarithm of the relative transmission curve; the minus sign at the right-hand side of equation (2.6) is already included.

with the plasma. After the laser beam has passed through the lamp, it is converged to a parallel beam by a lens. Next it passes an interference filter and is detected by the diode array, which consists of 32 evenly spaced photodiodes. The detector channel is converted into a lateral position and corrected for nonlinearities. Each detector channel corresponds to a unique lateral position in the lamp burner. The lamp is translated in height in steps of 0.5 mm to measure the density at different axial positions. In this way a two-dimensional mapping (lateral and axial) is obtained.

To obtain the spatially dependent dysprosium density first, for every position, the spectrally resolved relative transmission curve (shown in figure 2.7) is measured by taking the ratio of the transmitted laser intensity with the lamp on (corrected for the lamp emission) and off. In order to obtain the lateral dysprosium density, the logarithm of the transmission curve is fitted assuming a Lorentzian line shape (figure 2.8). The

measurement and fit fully coincide; no difference is seen. The area under the Lorentz curve is proportional to the line-of-sight (column) density of the dysprosium [43, 47]:

$$n_{\text{col},q}(x) = \int_{-\frac{1}{2}d(x)}^{\frac{1}{2}d(x)} n_q(x, y) dy, \quad (2.4)$$

where  $n_q(x, y)$  refers to the local dysprosium density of level  $q$  at position  $(x, y)$  in the plasma and  $d(x) = 2\sqrt{R^2 - x^2}$  corresponds to the line-of-sight boundaries at lateral position  $x$  (see figure 2.6). The relation between the area under the Lorentz curve and the column density can be determined using the Lambert-Beer law for absorption:

$$\frac{dI_\nu(s)}{ds} = -\kappa(\nu, s)I_\nu(s), \quad (2.5)$$

where  $I_\nu(s)$  is the spectral intensity of the laser beam (in  $\text{W m}^{-2} \text{sr}^{-1} \text{Hz}^{-1}$ ) and  $\kappa(\nu, s)$  the absorption coefficient ( $\text{m}^{-1}$ ) at frequency  $\nu$  at location  $s$ . After using the relation  $\kappa(\nu, s) = Sn_q\phi(\nu, s)$  with  $\phi(\nu, s)$  the line shape and integration over the frequency  $\nu$  one obtains:

$$\int_0^\infty \ln\left(\frac{I_{\lambda,d}(x)}{I_{\lambda,0}(x)}\right) d\lambda = -\frac{S\lambda^2}{c} n_{\text{col},q} = -2\frac{S\lambda^2}{c} \int_x^R \frac{n_q(r)}{\sqrt{r^2 - x^2}} r dr. \quad (2.6)$$

Note that by this technique the result is independent of the actual line shape.<sup>3</sup>

Finally the measured column density data are converted into a radial density profile [29, 48, 49]. In order to minimize errors in the central region we choose to approximate the radial density profile by a polynomial series:

$$n_q(r) = a_0 + \sum_{n=2}^{\infty} a_n r^n \quad \text{for } r \geq 0. \quad (2.7)$$

The term  $a_1 r$  is omitted because of the derivative of the dysprosium density at the axis of the burner should be zero. Using a least-square fitting procedure to the measured data the column values  $a_n$  are obtained and the radial profile is constructed.

Using this approach the density is independent of the actual line shape and depends linearly on the accuracy of the line strength  $S$  only.

## 2.4 Results

### 2.4.1 Lateral and radial profile

The lateral atomic dysprosium column density profile and the reconstructed radial profile 2 mm above the lower electrode of the lamp (151 W) are shown in figure 2.9. For fitting the radial profile, the terms until  $n = 6$  are used (equation (2.7)).

<sup>3</sup>The width of the Lorentzian profiles may vary along the line-of-sight. After integrating over the line-of-sight we again obtain a Lorentzian profile, where the area under curve—and thus the density—might be underestimated by 10–20%.

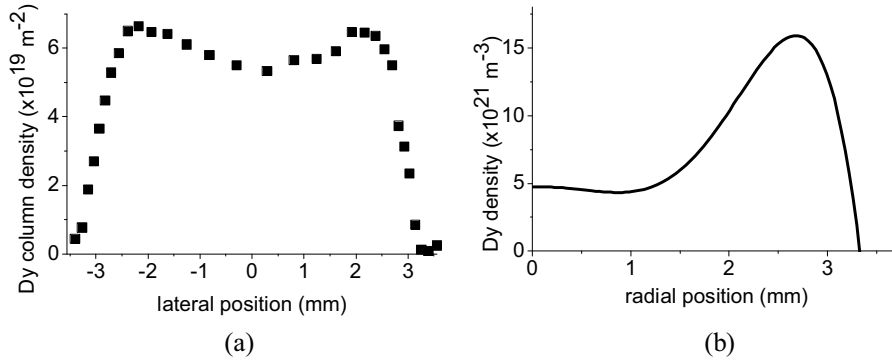


**Figure 2.9:** (a) Lateral dysprosium column density and (b) radial dysprosium density at 151 W; 2 mm above the lower electrode.

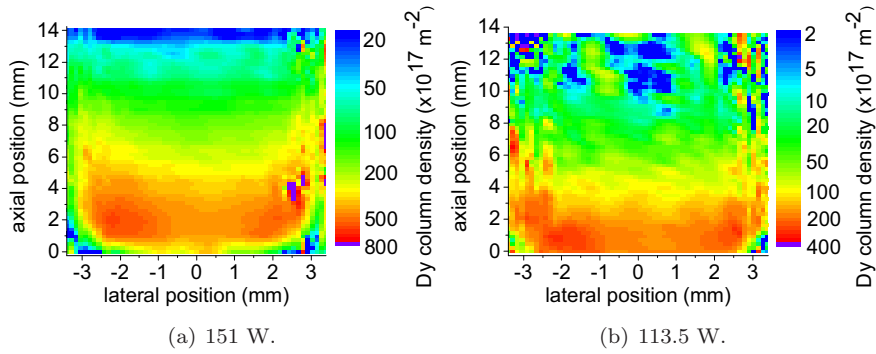


**Figure 2.10:** Two-dimensional profile of atomic dysprosium column density for (a) 151 W and (b) 113.5 W. The axial position of 0 mm is just above the lower electrode.

In figure 2.9(b) we see a hollow profile; this is in agreement with the theory (section 2.2.1). Atomic dysprosium is mainly present in a region around the central parts of the lamp (off-axis maximum), where the  $\text{DyI}_3$  molecules are fully dissociated. Close to the centre the temperature is even higher than at the off-axis maximum, resulting in lower overall densities and a partial ionization of the atomic dysprosium.

Around  $r = 1$  mm a small minimum is seen; this is an artifact caused by the limited number of lateral data points and the resulting incomplete reconstruction of the radial profile.

The order of magnitude of the dysprosium density ( $10^{22} \text{ m}^{-3}$ ) corresponds with expected values based on the cold spot temperature of  $\text{DyI}_3$  of  $\sim 1100 \text{ K}$  [29, 43].

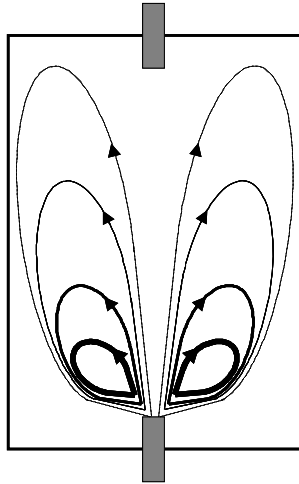


**Figure 2.11:** Representative flow lines of atomic dysprosium of what is believed to exist in the burner. The thick lines give a high dysprosium density whereas thin lines give a low density.

### 2.4.2 Two-dimensional profile

The two-dimensional profiles of the dysprosium column density of the lamp at 151 W and 113.5 W are given in figure 2.10. The curve in figure 2.9(a) corresponds to the horizontal line located at axial position 2 mm in figure 2.10(a).

The detection limit of the absorption measurement is around  $2 \times 10^{18} \text{ m}^{-2}$  as is seen in the top of figure 2.10(b). Near the bottom one sees that the column density gets low towards the wall. This is because of the arc contraction at the electrode. Furthermore the burner is not exactly cylindrical; the bottom area of the burner is somewhat curved (see figure 2.4).

The structure of the two-dimensional dysprosium column density in figure 2.10 is also remarkable. The dysprosium column density right at the centre is lower than the dysprosium column density close to the centre. When convection (upward in the centre; downward near the wall) and diffusion (direction towards the wall) are combined, the flow lines of atomic dysprosium look like figure 2.11, which qualitatively explains the observed structure.

### 2.4.3 Axial segregation

To obtain the axial segregation parameter  $\lambda$ , the measurements shown in figure 2.10 are converted into a radially averaged profile.

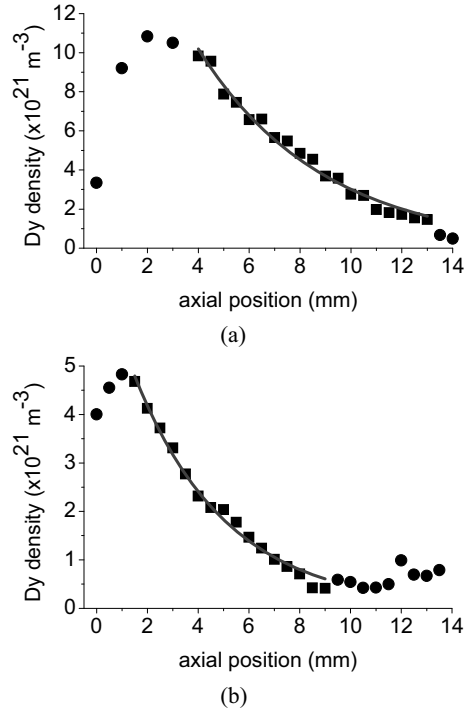


**Figure 2.12:** Dysprosium density as a function of axial position in the lamp (0 mm is just above the lower electrode). For the radial fit only  $a_0$  (equation (2.7)) is taken into account. The segregation fit (equation (2.3)) is only applied to the square dots. The segregation parameters for two different input powers are (a) 151 W:  $n_{\text{Dy},0} = (2.3 \pm 0.1) \times 10^{22} \text{ m}^{-3}$ ;  $\lambda = 0.20 \pm 0.01 \text{ mm}^{-1}$ ; (b) 113.5 W:  $n_{\text{Dy},0} = (7.2 \pm 0.2) \times 10^{21} \text{ m}^{-3}$ ;  $\lambda = 0.28 \pm 0.01 \text{ mm}^{-1}$ .

In figure 2.12 the atomic dysprosium density is shown as a function of axial position for 151 and 113.5 W. For both curves an exponential function is fitted according to equation (2.3) and the segregation parameters  $\lambda$  are obtained. The fit is not applied to the round dots; here deviation is present because of the electrodes and the not fully developed arc. The radial segregation at 113.5 W is larger ( $\lambda = 0.28 \pm 0.01 \text{ mm}^{-1}$ ) than at 151 W ( $\lambda = 0.20 \pm 0.01 \text{ mm}^{-1}$ ).

As already mentioned in the theory, the convection speed increases with increasing power. An explanation for the decreasing value of the segregation parameter  $\lambda$  with increasing power is that we are at the right part of the Fischer curve (figure 2.3); this agrees with previous findings on this lamp (parabolic flights where it is observed that the segregation decreased during a quick changeover to a  $1.8g$  hyper-gravity situation [43]).

## 2.5 Conclusions

The radially and axially resolved absolute number density of atomic dysprosium in a HID lamp was measured by means of laser absorption spectroscopy; this has been performed for two different input powers (113.5 and 151 W). The order of magnitude of the atomic dysprosium density is about  $10^{22} \text{ m}^{-3}$ .

The radially resolved atomic density measurements show that there is a hollow density profile with a maximum in the Dy density between the centre and the boundary of the plasma. In the outer parts of the lamp molecules dominate, while the centre is depleted due to ionization of dysprosium. Furthermore the overall density decreases towards the centre because of the higher temperature.

Due to diffusion and convection there is a strong axial segregation in the lamp. Apart from the electrode regions the average axial dysprosium density follows the theoretically predicted exponential dependence, and corresponding segregation parameters have been found:  $\lambda = 0.28 \pm 0.01 \text{ mm}^{-1}$  at 113.5 W and  $\lambda = 0.20 \pm 0.01 \text{ mm}^{-1}$  at 151 W. This shows that the lamp is operating at the right-hand side of the Fischer curve (more power means more convection and lower segregation). In the future a more careful analysis of the two-dimensional data will be compared to a numerical model of the lamp.

## Acknowledgements

The authors are grateful to J.J.A.M. van der Mullen and M. Haverlag for the discussion about the theory of the lamps, M. van Kemenade for his contribution to developing the measurement method and Senter-Novem (project EDI 03146) for funding the research.